CORPUS PUBLISHERS

Journal of Mineral and Material Science (JMMS)

ISSN: 2833-3616

Volume 4 Issue 2, 2023

Article Information

Received date : May 05, 2023

Published date: May 17, 2023

*Corresponding author

Digby Macdonald, Departments of Nuclear Engineering and Materials Science and Engineering, University of California at Berkeley, Berkeley, CA 94702-1730, USA

Key Words

Corrosion; Metallic aluminum; Electrochemical; Cracking; Resistance

DOI: 10.54026/JMMS/1060

Research Article

Observation of the Coupling Current During Stress Corrosion Cracking of Aluminum Alloy 5083

Krystaufeux Williams[1], Robert Bayles[2] and Digby Macdonald[3*]

[1]Former Employer - Center for Corrosion Science and Engineering, Naval Research Laboratory, Current Employer, IDA, Alexandria, VA

[2]Retired - Center for Corrosion Science and Engineering, Naval Research Laboratory, Current Employer: Excet, Inc, Springfield VA, USA

[3]Departments of Nuclear Engineering and Materials Science and Engineering, University of California at Berkeley, Berkeley, CA 94702-1730, USA

Abstract

A unique fracture mechanics device was created to allow for simultaneously measuring the load and localized electrochemical potential gradients in AA5083 bend bars. For the first time, periodic Scanning Vibrating Probe (SVP) maps were collected in order to obtain a full view of the coupling current, (which can be deduced from measured potential gradients) that emanates from an anodic crack tip. As a result of mapping the current density over a wide surface area compared to the area of the notch and crack tip, clarification is given on whether or not the external surfaces of an alloy or any other metal that experiences Stress Corrosion Cracking (SCC) play a role in crack growth. The SVP maps clearly show the anodic and cathodic potential gradients of a growing crack (resulting from SCC) in an AA5083 fracture mechanics specimen while the stress intensity increases. The notch and crack-tip remained anodic throughout most of the obtained scans for sensitized and as-received specimens. Furthermore, a coupling effect is observed on sensitized specimens even at low fracture toughness values in sensitized specimens under load for longer periods of time (> 1 week). These higher resolution maps captured during the crack growth process give more insight to the SCC phenomenon and the electrochemical mechanisms of crack growth in AA5083 and other alloys.

Introduction

Although several different alloys undergo Intergranular Stress Corrosion Cracking (IGSCC), they normally experience the phenomenon by different mechanisms. The main concern of the research mentioned in this paper is the IGSCC phenomenon occurring in sensitized AA5083. However, some innovative experimental approaches that were discovered during a prior study with 304 SS alloy in a boiling water reactor primary coolant environment that shed light on the IGSCC of the alloy of concern. The idea on monitoring the coupling current, if it exists and is measurable, proves useful insight to other alloy systems undergoing IGSCC, such as the mentioned AA5083. The construct of the prior research is described below. Based on the theory of differential aeration set forth by UR Evans, Macdonald and coworkers posited that a Coupling Current (CC), which is a current that flows from within a localized corrosion event (e.g., crevice, crack, pit, etc…) to the external surface as a result of the coupling between the internal and external environments, must exist during SCC of 304 SS alloy in a boiling water reactor primary coolant environment [1-6]. The seminal research performed by Macdonald, et al. showed that a time-based measurement of the Coupling Current (CC) could be made by mounting external cathodes within a few hundreds of microns of an electrically insulated fracture mechanics test specimen [1-6]. Once the load was applied to the specimen exceeding the critical stress intensity for crack growth under Mode I loading (KISCC), they observed that current flowed from the freshly exposed alloy in the crack-tip to the external cathode. Macdonald and coworkers [1-6] expected the CC to flow from the crack tip to the nearest external surface to the growing crack. Alternatively, other researchers suggested that if this CC exists, some or all of it can be extinguished within the confines of the crack mouth [7,8]. CC extinguishing in the confines of the crevice, according to the referenced authors, is based on the dynamics in the interior of the crevice geometry over long periods of time leading to micro-crevice formation in the internal environment of the crevice, or even a reverse crevice corrosion phenomenon where the external surfaces, in the case of non-passive metals such as Cu, corrode and the crevice is passive [7,8].

However, it is to be noted that a substantial portion of the CC must be annihilated on the external surface in order to maintain the crevice solution sufficiently aggressive (low pH, high [Cl^-]) to maintain crack growth. Also, if the coupling current was consumed inside the crack to produce hydrogen, only a small fraction of the coupling current would result in gas-flooding of the cavity, because of the large differences in the molar volumes of metallic aluminum and gaseous hydrogen. Thus, although some gas emission from the crack is observed, one concludes that only a small fraction (possibly less than 1 %) of CC is consumed within the cavity. Because of the existence of CC in alloys subject to SCC as reflected in these seminal studies, a testing apparatus was developed to determine if this CC may be measured with spatial resolution. There has been a considerable amount of effort put into understanding the mechanisms of Stress Corrosion Cracking (SCC) for particular alloys as each one has its own susceptibility. In this article, the focus is on SCC of AA5083. 5XXX series aluminum alloys experience sensitization due to exposure to moderate temperatures (50 °C) for long periods of time to high temperatures (175 °C) for shorter periods. Sensitization for this alloy occurs as a result of the formation of a Mg-rich β phase – Al_3Mg_2 that forms on the grain boundaries. Upon exposure to the temperature profiles discussed above, the β phase forms as a result of the diffusion of Mg to the grain boundaries where the intermetallic Al_3Mg_2 is formed. The β phase dissolves preferentially because it has a more negative corrosion potential than the bulk aluminum matrix.

Hence, cracking can proceed along these grain boundaries without as much resistance as an as-received allow with the same load applied. The work in this paper expands the research efforts mentioned above by obtaining, for the first time, in-situ positional potential maps used to infer the CC using a Scanning Vibrating Probe (SVP). Although the research focuses on shedding light on the mechanisms of SCC in AA5083, it can be universally applied to different alloy systems providing spatial maps throughout the stress corrosion crack growth process. Once it is determined whether the CC can

be resolved spatially, then differences in the spatial maps between the sensitized and the as-received specimens of AA5083 may be evident. Further, there was also a wealth of information for the fracture mechanics community as a result of the experiments performed including the ability to monitor stress corrosion, and other types of crack growth, in-situ. Finally, the issue of whether or not any localized corrosion current, or CC, exists on the external surface is resolved.

Obtaining Spatially-Resolved Potential Information

If a CC does indeed flow, as interpreted by the SVP potential maps, from an anodic crack tip to the external surface such that it may be measured on the external surfaces of the specimen, one should expect a localization of both the anodic and cathodic regions to appear on the scanning plane above the surface of the specimen as the sample approached KISCC. Furthermore, the local CC should flow from an anodic crack-tip to some cathodic region on the surface near the notch (see the following figures in this section). It could also be expected that in heavily sensitized specimens (Degree of Sensitization-DOS≥ 30mg/cm^2), more current would flow from the anodic region to the cathodic region (represented by intensity of a region measured by the SVP), when compared to the scans of the as-received samples (DOS≤ 4mg/cm^2) because more of the β phase is presented as the heavily sensitized specimen cracks. During SCC, the β phase eventually experiences anodic dissolution against the as-received AA5083 matrix metal. Although both mechanisms were posited to occur simultaneously for specimens with lesser DOS levels (lightly sensitized), in S.K.-Lee's recent summary of reports on crack growth mechanisms, he explained the consensus of those authors researching SCC of Al-Mg alloys that the HIC mechanism strongly influences growth through the alloy matrix (between discrete β particles) in lightly sensitized alloys (low DOS values) [9,10]. As the crack propagates through the β formations or along the interface of the grain boundary itself, the AD mechanism was considered to be more prevalent, since the β phase has a more negative potential than the Al matrix [9,10]. Research performed by Goswami, et. al., demonstrated though transmission electron micrographs that fully sensitized specimens (exposed to 175 °C for 240 hours) had continuous coverage of β phase on the grain boundary [11]. Therefore, it is expected that based on observations from the mentioned studies, Intergranular Stress Corrosion Crack (IGSCC) growth through a fully sensitized specimen with complete coverage of β phase on the grain boundaries should result in a more continual AD mechanism [9-11].

A more dominant HIC mechanism for crack advance may not experience the same increase in the CC because only a small fraction of it goes to produce atomic H. Most of the CC goes to balance differential aeration. The rate of production depends on the pH and the local potential at the crack tip must be sufficiently negative to produce H [9,10]. Nevertheless, in either mechanism of crack advance, failure still occurs sooner for sensitized materials due to the presence of the continuous β phase particles along the grain boundaries of the alloy (shown in the later sections). Furthermore, it was expected that at the onset of subcritical crack growth, a sharp increase in the coupling current/potential should be observed because of the introduction of newly exposed alloy to the solution. It was also likely that the combination of these mechanisms depends on the degree of sensitization as put forth by Holtz et al., and by Gao and Crane [11-13].

Experimental Setup

AA5083 material was obtained from Alcoa, Inc. in Pittsburgh, PA., as 1.91 cm (0.75 in.) thick rolled plates. Bend bars were cut from the plate that were the same thickness of the plate, 25.4 cm (10 in.) long and 3.81 cm (1.5 in.) thick. Specimens were in the T-L orientation with respect to the wrought plate. As-received and sensitized AA5083-H116 bend bars (0.75" thick x 10" long x 1.5" wide) were prepared for testing to determine the stress intensity for stress corrosion cracking in a four-point bending (pure bend) arrangement using a loading scheme as suggested by either ASTM F1624 – 12 or ASTM F1624-12, as well as to simultaneously monitor the CC utilizing the SVP [14,15]. In this study, a total of four sensitized bend bars were heat-treated by holding them at a temperature of 175 °C for 14 days and the effect of the heat treatment can be measured and analyzed using the techniques from ASTM G-67 [16]. DOS values were not measured directly, but determined from the heat treatment exposure temperature and time according to the referenced methods by Goswami, et. al. [12]. The expected DOS value for the fully sensitized specimens was 40-50 mg/cm^2. For as-received specimens, the expected DOS was ≤ 4 mg/cm^2. The experimental setup also involves a four-point bending fracture mechanics testing apparatus that was used to apply a load through a pure bending moment. The apparatus has been uncommonly arranged to lie on its side (horizontally), such that the direction of crack growth is parallel to the lab bench surface. Figure 1 shows the arrangement of the sample and the critical apparatus components. More traditional fracture machines are arranged vertically so that the load is applied in a direction perpendicular to the surface of the lab bench surface. Bend bar specimens were lying on the test machine in such a way that the crack on one face of the specimen was visible when viewed from above (the perspective of the SVP instrument). A 0.06 M NaCl solution was placed in a plastic container such that only the sawed chevron notch, the crack and the immediate middle section of the bar (approx. 2") was exposed.

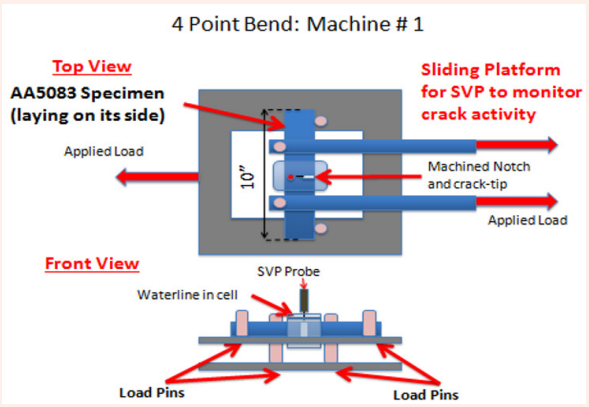

Figure 1: Schematic of the experimental setup demonstrating the approach to concurrent CC monitoring and fracture mechanics testing.

The experiment was designed in order to obtain electrochemical information above the sample as the load was held at incremental steps or while continuously increasing. Hence, an as-received specimen of AA5083 bend-bar was prepared for simultaneous loading and localized electrochemical testing utilizing a commercial SVP provided by Princeton Applied Research (now Ametek, Inc.). The probe was designed to vibrate in the z direction (in and out of the page on Top View of Figure 1) only. For all experiments, a constant probe height of 100±20 µm was maintained between the probe and the surface being scanned. Figure 2 shows the region above the samples where the probe is vibrating, obtaining signals, and rastering. Initial experiments were performed to understand the signal orientations as they related to the actual surface that was scanned by the SVP probe. A thin wire (on the order of 1 mm) of Mg was inserted into the scanning area to establish the nature of the signals (anodic/cathodic) measured by the SVP (Figure 2). Samples were immersed in 0.06 M NaCl solution as a compromise between the realistic seawater equivalent concentrations (0.6 M NaCl) and the optimal concentration for the best SVP resolution (on the order of mM of NaCl). Since Mg is a more active metal than aluminum, measurements taken above the Mg wire will be anodic as compared to the potentials obtained above the bulk alloy (Figure 2). Therefore, it was concluded that any additional, similarly oriented potentials (depending on the settings of the SVP as they can be set as negative or positive) from the same sample were also anodic. For the remaining experiments performed, anodic signals were set (utilizing the software to set the SVP's electrometer) to be negative (darker colors in the SVP potential maps shown below).

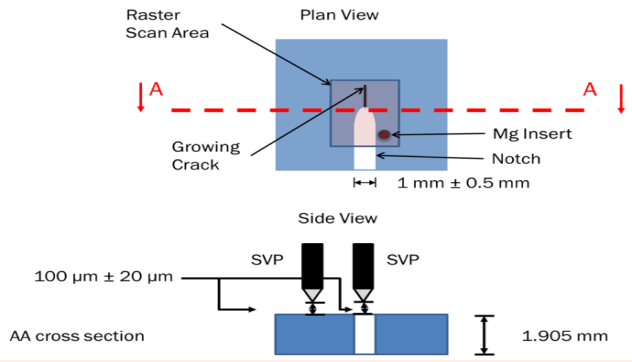

Figure 2: Section (plan view at the top and cross-section view at the bottom) of the as-received/unsensitized bend bar in test using the orientation of the obtained SVP scans presented. The increasing y direction is parallel to the growing crack increasing in the up direction on this page.

Specimens were pre-cracked after introducing a band-sawed chevron notch using procedures described Annex A2 of ASTM E399 [17]. Initially, the specimens were placed in a separate 3-point bend arrangement where a cyclic load ratio of R=0.1 was imposed. The MTS machine for performing the pre-cracking was placed in load control with a KI set to about 20% of KIC. A computer program was implemented using LabVIEW software to automatically shed the load as the crack grew from about 0.4 a/W (measured using the compliance equations in ASTM E399) to about 0.5 a/W. Samples were loaded at a rate of approximately 20 Hz. Finally, once the stress intensity reached about 0.5% of KIC, the program was stopped and the SCC portion of the testing began. Since the fatigue pre-crack length of fracture mechanics specimens was known (bend bars were pre-cracked in a separate 3-point bend arrangement) from the compliance relationships in ASTM E399, as well seen in the light and scanning electron micrographs of post-mortem fracture surfaces, that length was used in the present study to determine the KISCC [17]. Table 1 contains the parameters for the specimens tested.

Table 1: Description of the experimental parameters for each of the specimens described in the paper.

Sample #	Treatment	Tests
U003	As-received	Continuous load from 200 lbs. (890 N)
S004	Sensitized at 175°C for 14 days – DOS = 45 mg/cm^2	Constant load = 200 lbs. (890 N)
S005	Sensitized at 175°C for 14 days – DOS = 45 mg/cm^2	Continuous Rising load from 200 lbs. (890 N)
S006	Sensitized at 175°C for 14 days – DOS = 45 mg/cm^2	Continuous Rising load from 700 lbs. (3114 N)
S007	Sensitized at 175°C for 14 days – DOS = 45 mg/cm^2	Incrementally increasing load from 500 lbs. (2224 N)

Results and Discussion

Following dissolution of the Mg wire (Figure 3), anodic signals appeared in the region of the notch and pre-crack of the unsensitized specimen, as shown in Figure 4. The more electronegative signals are located towards the opening of the notch as opposed to the crack-tip, which had not started growing yet. The load was continuously increasing at a rate of about 50 lbs./hr., see Figure 5. A few scans were performed before the load ramping began and there was already increasing activity within the notch of the specimen, due (presumably) to crevice corrosion (see Figures 4 & 6). When the load reached about 500 lbs., a cathodic region (brighter colors on the local potential gradient scale) was observed in the upper right corner of the scan (Figures 6 & 7). The appearance of this brighter cathodic region and the dark anodic region within the notch in Figures 6 & 7, unequivocally demonstrates the flow of ionic current (which refers to the positive ions exiting the crack to deposit on the external surface) from the notch to the external surface of the specimen (i.e., demonstrates the existence of the coupling current). Regions of coupling current originate from an anodic crack-tip (distinguishable from the other scanned regions by a darker brown section extending from the top of darker slit in the center of Figures 8a & 8b where the notch was located) and are adjacent to a highly cathodic region. However, any additional consistently dark zones (i.e., anodic regions), such as the notch or other sensitized patches of grains on the surface of the sample (see next section) were also assumed to produce coupling current (Figures 4 & 6-11). Other topological features on the sample were expected not to have affected the scan, since the probe does not make contact with the specimen and since the top surface was abraded with 600-grit SiC paper and rinsed before testing and the SVP probe is positioned 100±20 µm above the sample surface. The results for the initial sensitized specimens studied are shown in Figures 9 through Figure 11. The sensitized AA5083 specimens were characterized by highly localized and sharp anode and cathode regions meeting at the crack-tip. The CC is discovered to grow to a peak for the opening of the notch and pre-crack and then diminish with time (comparing the sharp CC localization SVP map taken at the lower load in Figure 9 to the broader CC in the map taken at a higher load in Figure 11). Afterwards, the CC grew again after the KISCC value was reached. Based on the performed by Gross and Srawley, the calibration for determining stress intensity for a pure bend specimen was $Y^2_{ns} = 139\,a/W - 221\,(a/W)^2 + 783\,(a/W)^3$, where $Y^2 = K^2 B^2 W^3 / M^2$, K was the stress intensity, B was the specimen thickness, W was the notch depth, M was the specimen bending moment at mid-span (M=PS/4), and a was the crack length [18]. From measurements made on light micrographs and physical parameters, we found a=0.0168m (0.661 in), W=0.039m (1.55 in.), B=0.19m (0.75 in.), and W=0.039m (1.54 in.). With a span of S=0.2032m (8 in.) and an applied load just before subcritical crack growth of P= 3207.17 N (0.721 Kips), the moment was M=162.92 N-m (1.442 in.-kips). Using a K calibration and parameters for the pure-bend specimen mentioned , a K_{ISCC} = 9.82 MPa-m$^{1/2}$ (8.94 ksi-in$^{1/2}$) was obtained. This growth occurred much sooner (at a lower value of the load) than in the unsensitized counterparts. A representative SEM image for specimens experiencing a ductile tearing that takes place in as-received specimens was compared to one experiencing flat, and brittle failure as in the fully sensitized specimens. These SEM micrograph images are compared and shown in Figure 12.

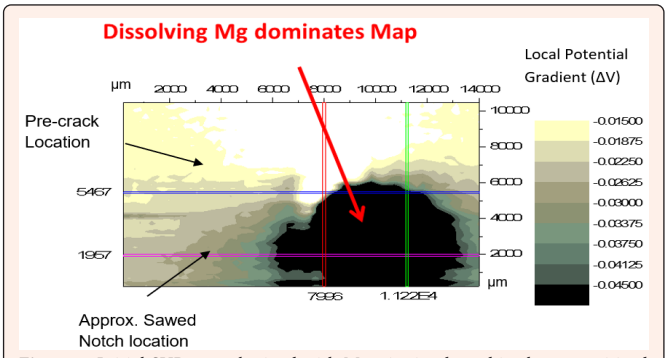

Figure 3: Initial SVP map obtained with Mg wire implanted in the unsensitized sample to establish signal orientation with active elements on the sample.

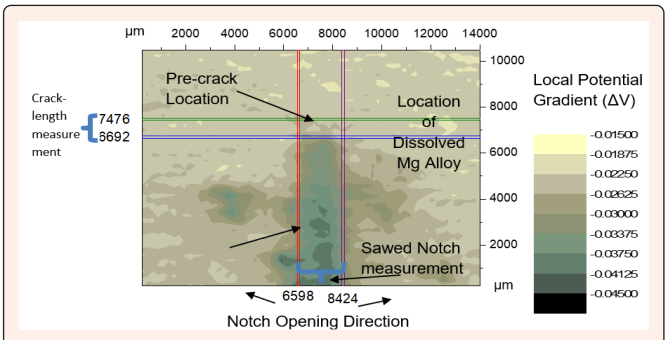

Figure 4: Accompanying potential map for the unloaded unsensitized sample in test as shown in Figures 1 and 2. The map was obtained following the dissolution of the Mg insert. Horizontal and vertical parallel lines were used to measure the width of the notch and the crack-length (as indicated by SVP activity only), respectively.

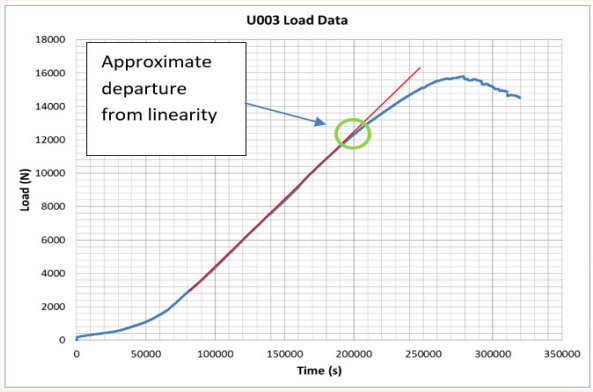

Figure 5: Loading profile for an unsensitized AA5083 specimen (in blue) in 0.06 M NaCl with a superimposed straight line (red) to give a visual estimate of departure from the linear-elastic regime, or rather the onset of subcritical cracking. CC potential maps were collected before and after the onset of crack growth.

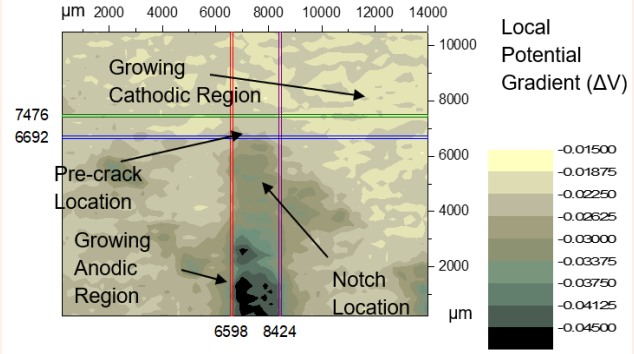

Figure 6: A follow-up scan of the unsensitized specimen (as-received), U003 with no load. The activity in the notch increased since the first scan was acquired.

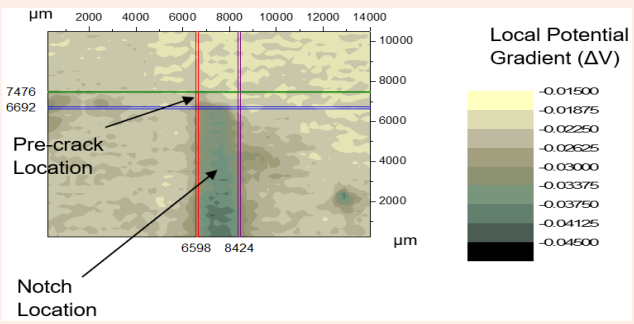

Figure 7: Continued scanning of specimen U003 (as-received). Load reached a value of approximately 500 lbs. (2224 N) approximately 20 hrs. after the scan in Figure 6.

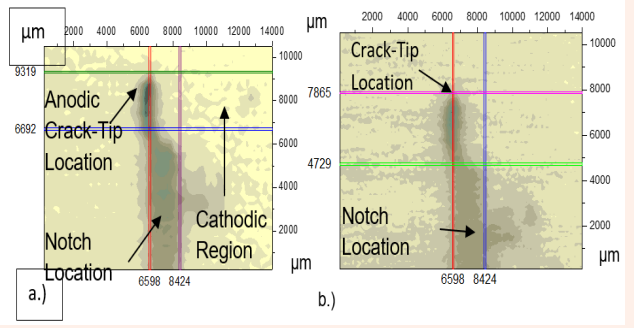

Figure 8: a.) At a load of approximately 1750 lbs. (7784 N), the sample (U003) has opened up to the position of the pre-crack and the crack-tip has become anodic. b.) The load has increased beyond K_{ISCC} and the crack has arrested and developed a large plastic zone. The sample was warped as a result and the notch was curved rather than straight. The colored local potential gradient scale is the same as in Figures 4, 6, and 7.

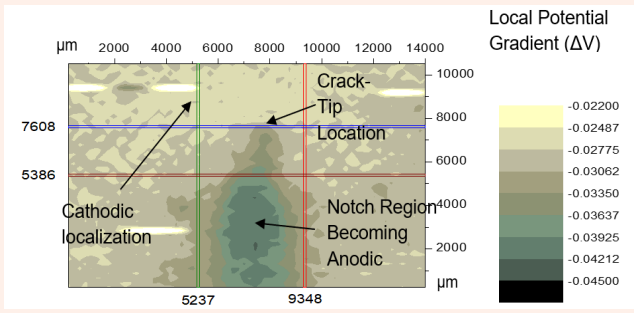

Figure 9: An SVP scan of sensitized specimen S006 at an initial load of about 700 lbs (3114 N). The pre-crack has opened up slightly as a result of the load leading to the presence of CC. No crack growth expected at this stage. Note that the CC will exist for Intergranular Attack (IGA) even though no crack growth is occurring.

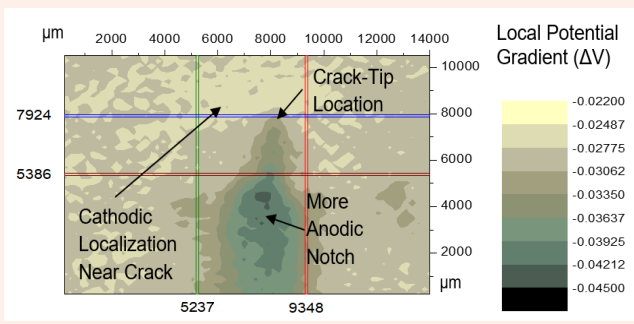

Figure 10: SVP scan taken after the initial loading discussed in Figure 9 where the pre-crack that is 2794 um deep is almost fully opened.

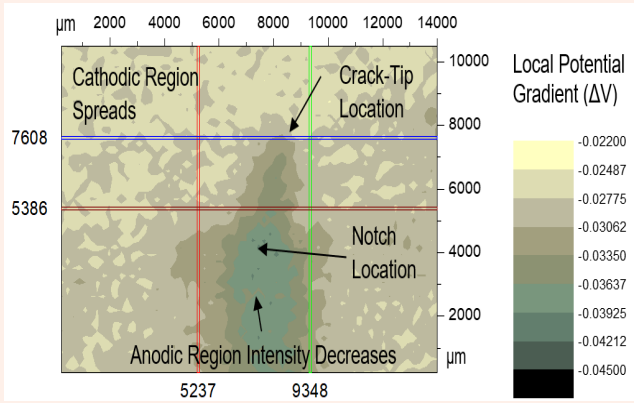

Figure 11: Decay in the CC is shown at a load of 910 lbs. (4048 N) before crack growth is expected to occur ($K_I \leq K_{ISCC}$).

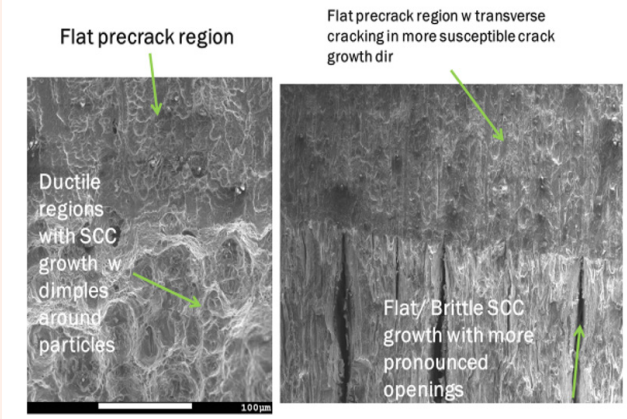

Figure 12: Figures show an SEM image of as-received specimen (left) that transitions immediately from pre-crack (upper portion) to ductile tearing (lower portion) in comparison to an SEM image of a sensitized specimen (right) that transitions from the flat pre-crack region (upper portion) to less flat region of intergranular SCC (lower portion).

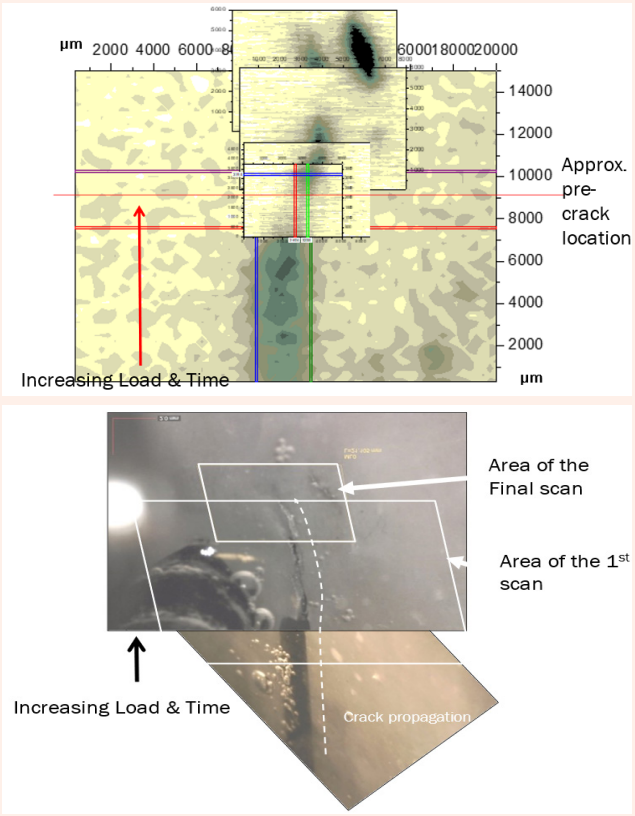

Figure 13: Comparison of a collage of SVP images with a similarly oriented collage of light microscope images.

A collage of SVP and light microscope images were compared to show (revealing the total regions scanned by SVP and comparing it to similar features in the light micrographs) how close the cc and actual crack shape were (Figure 13). One example of features in both the light microscope and SVP collages tracking closely is in the notched areas. The SVP scans of unsensitized specimens revealed a less localized cathodic potential region near the crack tip during crack growth (Figures 4 & 6-8). The crack-tips also appear to be less sharp when the crack experiences the highest value of stress intensity than the sensitized counterparts. The reason for the blunted crack-tip might be related to the development of a plastic zone that arrested the crack. Ultimately, some of these crack-tip shapes based on the SVP scans appeared to be connected to the different crack growth mechanisms between sensitized and as-received specimens. While the height of the probe was maintained constant even above the notch and crack-tip regions, there was still reason to believe that the z (height) component of the anodic potential SVP signals related to current passed between the crack-tip and external surface. The main reason involved increased intensity of cathodic regions on the external surfaces beyond the notch where the specimen appears to be relatively flat. Also, there was a transient nature of the anodic and cathodic SVP signals (signals increased with time before subcritical crack growth began and decayed with time a while after the KISCC is surpassed) revealing that while topology changes can lead to uncertainty in SVP signal, the obtained data related to local electrochemical phenomena.

Conclusion

The localized anodic and cathodic nature of crack growth in AA5083 was illustrated for the first time. Furthermore, clarification on the issue of whether the CC was annihilated on the external surfaces of specimens has been given [19]. When the SVP collected actual electrochemical phenomena, the changing of these maps over the course of the experiment verified the existence of coupling current on the external surfaces of the crack for which this setup was designed to expose and monitor. Considering the figures showing the SVP maps of the active crack-tips and their corresponding cathodic counterparts on the external surface adjacent to the growing crack, it may be possible to promote or arrest crack growth electrochemically in the external environment. If one can stop crack growth by adjusting the voltage of the specimen to a value below this theoretical critical potential, and if the critical potential that is predicted by the Coupled Environment Fracture Model (CEFM) then it should be possible to predict Crack Growth Rates (CGR) via the CEFM over the full range of potential, stress intensity factor, and solution conductivity, as described previously [13], because of the deterministic nature of SCC. Further calculation and analysis from the current density maps will be reported in future publications focusing on obtaining average growth rates while the load is held at different values.

Acknowledgement

The author gratefully acknowledges the US Naval Research Labortory (NRL) Student Career Experience Program for funding. The author also acknowledges Dr. Ronald Holtz at NRL for performing heat treatment of aluminum alloy specimens.

References

1. Soundararajan B, Macdonald DD (2004) Caustic cracking of AISI 4340 steel. Corrosion 2004 Paper No. 04572. NACE International, New Orleans, LA, USA.
2. Manahan MP, MacDonald DD, Peterson AJ (1995) Determination of the fate of the current in the stress corrosion cracking of sensitized type 304SS in high temperature aqueous systems. Corrosion Science 37(1): 189-208.
3. Zhou X, Balachov I, Macdonald DD (1998) The effect of dielectric coatings on IGSCC in sensitized type 304 ss in high temperature dilute sodium sulfate solution. Corrosion Science 40(8): 1349-1362.
4. Macdonald DD, Engelhardt GR, Balachov I (2008) Environment-induced cracking of materials. Elsevier, Amsterdam, Netherlands, pp. 55-92.
5. Gomez-Duran M, Macdonald DD (2003) Stress corrosion cracking of sensitized type 304 stainless steel in thiosulfate solution: I. Fate of the coupling current. Corrosion Science 45(7): 1455-1471.

6. Gomez-Duran M, Macdonald DD (2006) Stress corrosion cracking of sensitized type 304 stainless steel in thiosulphate solution. II. Dynamics of fracture. Corrosion Science 48(7): 1608-1622.
7. Lu L, Li X (2011) Corrosion products of reverse crevice corrosion of copper. Int J Min Met Mater 18: 320-324.
8. Kennell GF, Evitts RW (2009) Crevice corrosion cathodic reactions and crevice scaling laws. Electrochim Acta 54(20): 4696-4703.
9. Lee SK (2013) The coupled environment models for localized corrosions; Crevice corrosion and stress corrosion cracking. Doctoral Dissertation, Department of Materials Science and Engineering. The Pennsylvania State University, University Park, PA, USA.
10. Lee SK, Lv P, Macdonald DD (2013) Customization of the CEFM for predicting stress corrosion cracking in lightly sensitized Al–Mg alloys in marine applications. Journal of Solid State Electrochemistry 17: 2319-2332.
11. Crane CB (2013) Validation of the coupled dissolution-Hydrogen embrittlement mechanism of IGSCC in low temperature sensitized AA5083-H131. Doctoral Dissertation. University of Virginia, USA.
12. Goswami R, Spanos G, Pao PS, Holtz RL (2010) Precipitation behavior of the ß phase in Al-5083. Materials Science and Engineering: A 527(4-5): 1089-1095.
13. Gao J, Quesnel DJ (2011) Enhancement of the stress corrosion sensitivity of AA5083 by heat treatment. Metallurgical and Materials Transactions A 42: 356-364.
14. ASTM E1681- 03, E Committee (2008) Test method for determining threshold stress intensity factor for environment-assisted cracking of metallic materials. ASTM International, West Conshohocken, PA, USA.
15. ASTM F1624 - 12, F Committee (2009) Test method for measurement of hydrogen embrittlement threshold in steel by the incremental step loading technique. ASTM International, West Conshohocken, PA, USA.
16. ASTM G67 - 04, G Committee (2004) Test method for determining the susceptibility to intergranular corrosion of 5XXX series aluminum alloys by mass loss after exposure to nitric acid (NAMLT Test). ASTM International, West Conshohocken, PA, USA.
17. ASTM E399 - 90, E Committee (1991) Test method for plane-strain fracture toughness of metallic materials. ASTM International, West Conshohocken, PA, USA, pp.1-34.
18. Bernard G, Srawley JE (1997) Stress-intensity factors for three-point bend specimens by boundary collocation. SPIE Milestone Series MS 138: 256-268.
19. Evans UR, Bannister LC, Britton SC (1931) The velocity of corrosion from the electrochemical standpoint. Proceedings of the Royal Society of London. Series A, Containing Papers of a Mathematical and Physical Character, 131: 355-375.